water

MDPI

Article

WINDS Model Simulation of Guayule Irrigation

Matthew E. Katterman [1], Peter M. Waller [1,*], Diaa Eldin M. Elshikha [1], Gerard W. Wall [2], Douglas J. Hunsaker [2], Reid S. Loeffler [1] and Kimberly L. Ogden [3]

[1] Department of Biosystems Engineering, University of Arizona, Tucson, AZ 85721, USA; mkatterman@arizona.edu (M.E.K.); diaaelshikha@arizona.edu (D.E.M.E.); reidloeffler@arizona.edu (R.S.L.)
[2] USDA-ARS, Arid Land Agricultural Research Center, Maricopa, AZ 85138, USA; gary.wall@usda.gov (G.W.W.); doug.hunsaker@usda.gov (D.J.H.)
[3] Department of Chemical Engineering, University of Arizona, Tucson, AZ 85721, USA; ogden@arizona.edu
* Correspondence: pwaller@arizona.edu; Tel.: +1-520-440-5803

Abstract: The WINDS (Water-Use, Irrigation, Nitrogen, Drainage, and Salinity) model uses the FAO56 dual crop coefficient and a daily time-step soil–water balance to simulate evapotranspiration and water content in the soil profile. This research calibrated the WINDS model for simulation of guayule under full irrigation. Using data from a furrow irrigated two-season guayule experiment in Arizona, this research developed segmented curves for guayule basal crop coefficient, canopy cover, crop height and root growth. The two-season guayule basal crop coefficient (K_{cb}) curve included first and second season development, midseason, late-season and end-season growth stages. For a fully irrigated guayule crop, the year one midseason K_{cb} was 1.14. The second year K_{cb} development phase began after the crop was semi-dormant during the first winter. The second year K_{cb} value was 1.23. The two-season root growth curve included a growth phase during the first season, no growth during winter, and a second growth phase during the second winter. A table allocated fractions of total transpiration to soil layers as a function of root depth. With the calibrated tables and curves, the WINDS model simulated soil moisture content with a root mean squared error (RMSE) of 1- to 3-% volumetric water content in seven soil layers compared with neutron probe water contents during the two-year growth cycle. Thus, this research developed growth curves and accurately simulated evapotranspiration and water content for a two-season guayule crop.

Keywords: irrigation scheduling; model; evapotranspiration; soil water; root activity; cotton

Citation: Katterman, M.E.; Waller, P.M.; Elshikha, D.E.M.; Wall, G.W.; Hunsaker, D.J.; Loeffler, R.S.; Ogden, K.L. WINDS Model Simulation of Guayule Irrigation. *Water* **2023**, *15*, 3500. https://doi.org/10.3390/w15193500

Academic Editor: Guido D'Urso

Received: 4 September 2023
Revised: 27 September 2023
Accepted: 5 October 2023
Published: 7 October 2023

1. Introduction

The WINDS (Water-Use, Irrigation, Nitrogen, Drainage, and Salinity) model currently evaluates irrigation experiments and will potentially provide decision support for irrigated-crop management in the U.S. Southwest. This research calibrated the WINDS model for simulation of guayule irrigation.

Irrigated agriculture in the southwestern U.S. desert is beset by water shortages due to ongoing drought and reallocation of available water supplies to industrial and municipal uses [1]. Efficient crop water management practices and alternative low water use and drought tolerant agricultural crops with economic potential are needed [2]. Guayule (*Parthenium argentatum*, A. Gray) is the top alternative crop entering the crop mix in Arizona. It is a perennial shrub native to the Chihuahuan Desert that produces high-quality natural rubber, appropriate for manufacturing commercial-grade tires [3]. In addition, it produces resin, which has many potential applications, and bagasse, which can be converted to biofuel or high-density composite boards [4]. Guayule is normally grown for two years before the first harvest. It can be regrown and harvested in two to three-year cycles [5,6]. Guayule is a drought tolerant plant that survives high temperatures and limited amounts of water. Its acclimation to the arid desert environment gives it great resiliency, where it can produce rubber yields with as little as 500 mm of applied water per year [7] and

survive on just a few irrigations per year [8]. Previously, the conventional wisdom was that guayule rubber productivity was maximized when irrigation applications replace full crop evapotranspiration (ET_c) requirements, which are on the order of about 1500 to 1600 mm per year [9–12]. However, recent research [8] showed that rubber productivity (kg rubber/kg water) could be optimized with annual applications in the range of 700 mm/year. This makes it an attractive crop at a time when many farmers face water cutbacks.

Irrigation simulation models based on a soil–water balance (SWB) provide a means to improve irrigation scheduling decision-making and optimize irrigation water use [13,14]. Many daily SWB irrigation simulation models are available, including AquaCrop [15], CROPWAT [16], and SIMDualKc [17]. While various methods have been used to estimate the ET_c component of the SWB, current models [14] predominantly use the FAO56 single crop coefficient method [18] that computes ET_c as K_c times ET_o, where K_c is the crop coefficient and ET_o is the reference evaporation calculated by the standardized Penmen-Monteith equation using local weather data. The daily ET_c is computed more precisely by using the FAO56 dual crop coefficient procedures that separates K_c into its basal (K_{cb}, transpiration) and soil evaporation (K_e) factors [18]. Pereria et al. [19,20] provide standardized K_c and K_{cb} data for major agricultural crops, excluding guayule. Many others have derived crop coefficients for local environments based on measurements of actual ET_c [21–24].

Remote sensing indices can be integrated within the FAO56 dual procedures to provide real-time estimation of K_{cb} during the growing season [14]. Remote sensing has been used to estimate crop coefficients for cotton [25], wheat [26], vegetables [27] and sugar cane [28]. A recent study estimated daily K_{cb} from satellite data. [29]

Tractor-based systems enable site specific irrigation scheduling. Electrical resistance tomography was combined with satellite images and an FAO56 ET model to characterize orchard evapotranspiration [30]. Multiple sensors were deployed on a tractor to characterize spatially variable water content and other properties for site-specific irrigation [31].

Inexpensive soil sensors connected to the cloud have enabled automated irrigation scheduling [32–35]. Several drip irrigation companies offer automated irrigation scheduling with their proprietary soil sensors and irrigation controllers.

Irrigation scheduling can incorporate economic analysis to optimize water productivity and profit [36,37].

The WINDS (Water-use, Irrigation, Nitrogen, Drainage, and Salinity) soil–water balance model [38] is a research tool and irrigation scheduling app. This research was part of the calibration work for the model in the Sustainable Bioeconomy for Arid Regions (sbar.arizona.edu) guayule irrigation experiments. The data and simulations from this and other SBAR irrigation experiments are available at the public viz WINDS site (https://viz.datascience.arizona.edu/WINDS/, 10 September 2023). To view data from this experiment, click “Select a planting”, and choose “2018 Maricopa Guayule Flood 100% Average”, or any of the replicates, and chec k “Field Data”.

The WINDS model uses daily time-steps, employing a tipping bucket approach during infiltration events and Richards’ equation [39] between infiltration events. Previous research demonstrated that the Richards’ equation parameters (Mualem-Van Genuchten soil characteristics) have minimal influence in sandy loam soils, such as the soil in this research [38]. Almost all the soil flux between layers is accounted for in the tipping bucket model. The WINDS model calculates crop evapotranspiration with the FAO56 dual crop coefficient procedure. The WINDS model uses a root activity and root depth table to estimate soil water depletion as a function of depth and growth phase [38].

The overall goal of this research was to use data from a two-year guayule furrow irrigation experiment in central Arizona to parameterize the WINDS model for irrigation prediction and soil water simulation in layers. This research specifically used the Furrow 100 treatment, which was full replacement of ET to field capacity. Experimental methods are described in detail in [12,40,41]. The robustness of the calibrated curves was evaluated at six neutron probe access tubes in the F100 treatment.

2. Materials and Methods

On 20 April 2018, guayule (USDA AZ-2 germplasm) was directly seeded using a four-row planter in a 1.0 ha field at the University of Arizona Maricopa Agriculture Center (MAC) farm in Maricopa, AZ (33.07° N lat; 111.97° W long; 361 m a.s.l.). The field consisted of 18 plots, each containing 6 rows spaced 1.02 m apart and 6.1 m wide. After planting, the field was wetted daily using sprinkler irrigation for two weeks with total applied water of 284 mm to germinate and establish of the crop. Next, the plots were given a uniform flood irrigation treatment totaling 600 mm between May and June 2018. Afterwards, the irrigation study commenced on July 2018, employing differential irrigation treatments. In the furrow (flood) treatment, which is the subject of this research, there were 68 total irrigation events with 12 sprinkler germination events and 56 furrow (flood) irrigation events. Elshikha et al. [12,40] provided a complete description of the experiment.

The irrigation study utilized a split-plot experimental design with field location as the main plot and the specific irrigation treatments as the split-plots. The field was divided into three blocks, each containing six randomly assigned treatments. Each block consisted of five subsurface drip irrigation (SDI) treatments labeled as D50, D75, D100, D125 and D150 and one flood irrigated treatment known as F100. The field map outlining this split-plot design along with all F100 access tubes marked as R1–R6 are shown in Figure 1. Only the F100 access tubes are displayed in the map because that was the focus of this research, which focused on flood irrigation simulation. All other treatments were drip treatments. In the F100 treatment, water was applied when the soil water depletion reached 55%. Furrow plots (flood) were irrigated using an overflow rise valve at the end of each plot. The flow rate and water volume for furrow (flood) irrigations were measured with a calibrated in-line propeller water meter.

Irrigation timing and depth were based on measured soil water contents in the F100 treatment. Depletion was the product of layer thickness and the difference between field capacity and measured water content in each layer. Irrigation depth was the sum of depletions in all layers in the root zone. Procedures outlining the direct calculation of crop evapotranspiration (ET_c) between two soil moisture reading dates using the FAO 56 dual crop coefficient method [18] are described by [25].

Meteorological data was obtained from the Arizona Meteorological Network (AZMET; https://cals.arizona.edu/AZMET/index.html, 10 September 2023) [42] located at the MAC farm site. Weather parameters required for the WINDS model include daily minimum and maximum air temperatures, minimum relative humidity, wind speed, and daily precipitation. The AZMET station calculates daily reference evapotranspiration (ET_o) based on the ASCE standardized Penman–Monteith model [43].

The soil was a Casa Grande series (Fine-loamy, mixed, superactive, hyperthermic Typic Natrargids) [44].

Six 2.25 m long by 51 mm diameter galvanized steel access tubes were installed in three flood irrigation treatment plots. The neutron moisture meter (Campbell Scientific) measured soil–water content from 0.15 m to 1.95 m below the soil surface in 0.3 m increments. Soil moisture readings were taken at weekly or biweekly intervals from 7 August 2018 to 3 March 2020 for a total of 59 sampling dates. Volumetric soil water content (θ_v) is calculated from NMM standard counts (SC) and readings (C) along with probe slope (m) and intercept (b). The slope and intercept were derived from soil tests taken at three locations in the field. Separate slope and intercept values were calculated for the top layer due to its proximity to the surface. There were seven soil layers of 30 cm depth in the WINDS model, corresponding with NMM sampling depths. The upper layer was divided into the evaporation layer (layer eight), which was 0–11.5 cm, and layer seven, from 11.5 to 30 cm.

The WINDS model inputs for this research included irrigation, weather, root characteristics, canopy growth, crop coefficient and other crop growth parameters, wetted fractions, soil layers, ET fractions, and neutron probe measurements. Inputs are set up in database format. For example, a single irrigation page includes irrigation data for all experiments. For this experiment, the WINDS model had seven soil layers plus an evaporation layer

corresponding with Neutron Moisture Meter (NMM) water content readings for the soil profile. Primary soil parameters for this research were field capacity and permanent wilting point because the primary water transport calculation was with the tipping bucket model. Weather parameters were from the Arizona Meteorological Network (AZMET), which has a station within 200 yards of the experiment. Wetted fractions table specifies the fraction wetted in the horizontal direction, which was 1.0 for all layers with surface irrigation. The ET fractions table specifies the fractions of ET from each layer as a function of root depth. This table was parameterized based on observed wetting patterns. Further detail on WINDS model parameterization is in the Results section.

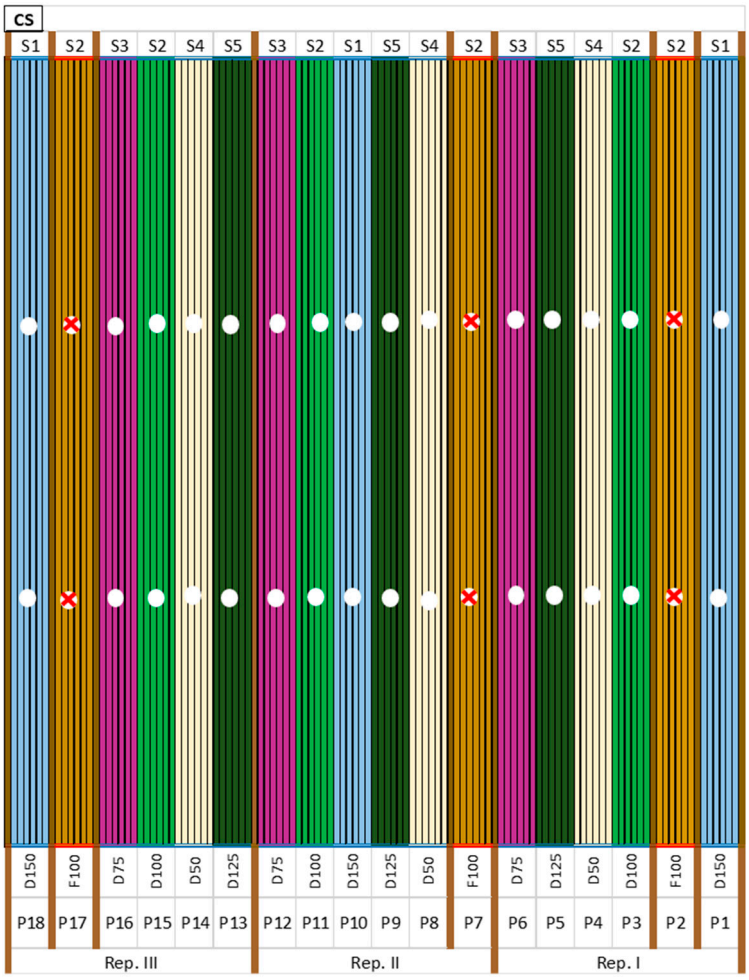

Figure 1. Map of guayule irrigation treatments at the MAC with two NMM access tubes per replicate. The D50–D150, and F100 replicates represent drip and furrow (flood) treatments, respectively. Neutron probe access tubes are represented by white circles. The six neutron probe access tubes in this research are marked with a red x.

In this research, the WINDS model was initially calibrated against the average of five neutron probe locations. One access tube was left out of the average because it had dramatically different soil characteristics in the lower layers. The WINDS model was then evaluated for each individual neutron probe access tube.

Manual measurements of plant height and canopy cover were conducted for nine plants per plot once every 30 days from June 2018 through March 2020. The measurements were used to calibrate the RGB estimations of canopy cover [40]. Figure 2 is an RGB image of the experiment. The three furrow replicates used in this research are marked. Two drone systems collected the RS data. The first was a Phantom 4 Pro V2.0 drone (DaJiang Innovations (DJI), Nanshan District, China). It collected RGB images 30–60 m above

the ground. Canopy cover was calculated from the RGB images through a hue, saturation and intensity (HIS) color space algorithm [45]. Weekly drone flights generated weekly averages for the interior of each plot.

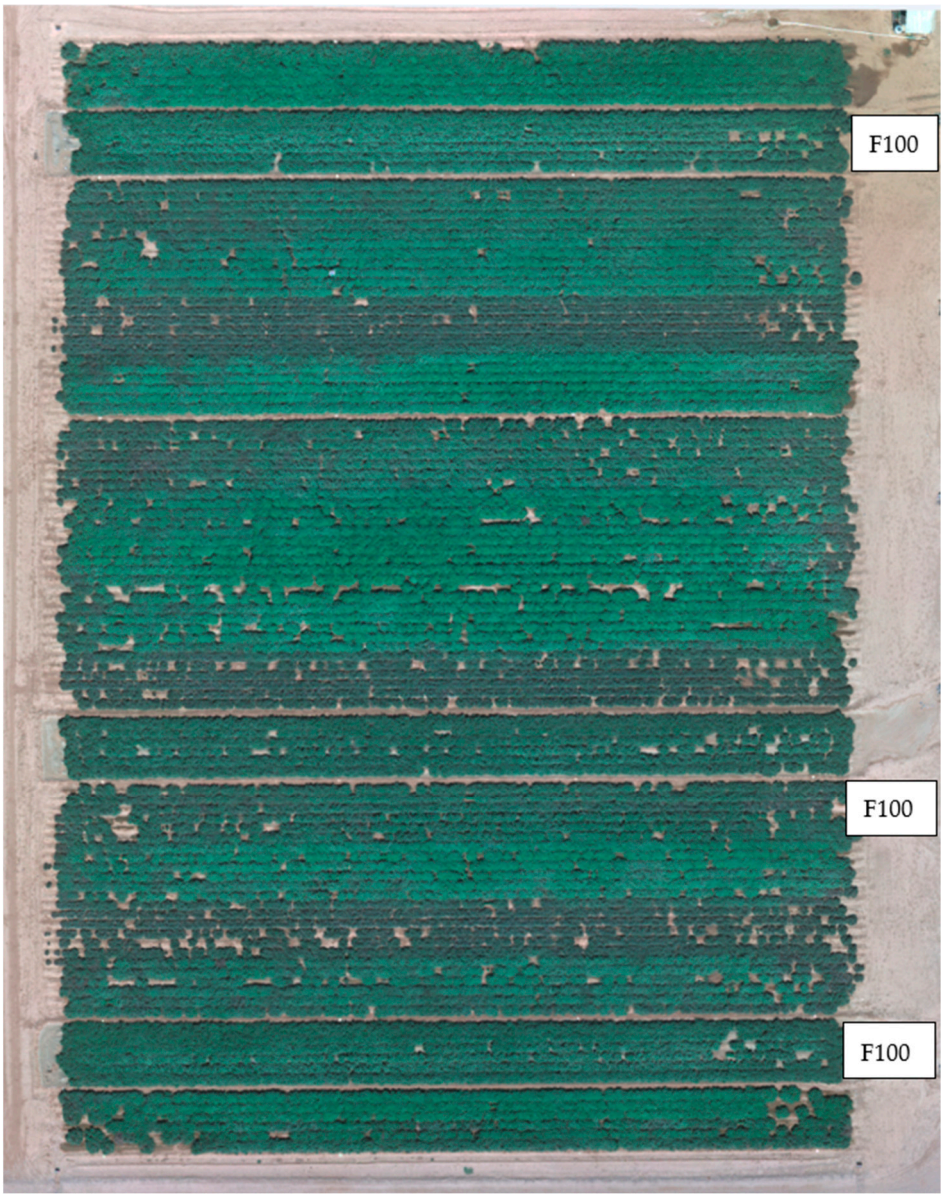

Figure 2. An RGB image of the guayule irrigation experiment at the Maricopa Agricultural Center with the three fully irrigated flood (F100) treatment plots marked. Two neutron probe access tubes were in each furrow plot. Image collected August 2019. Note that this figure has a different orientation than Figure 1, rotated 90 degrees counterclockwise.

The second drone system was an Inspire 2 (DJI, Nanshan District, China) that contained a multispectral MicaSense Altum sensor, which has five bands (Blue [475 nm], Green [560 nm], Red [668 nm], Red Edge [717 nm], Near Infrared [842 nm]) and a thermal infrared (LWIR) band [8000–14,000 nm]. Reflectance from the crop canopy (near infrared [NIR] and red [R]) allowed for the generation of a Normalized Difference Vegetation Index (NDVI) [46].

3. Results

This section presents the unique plant and root growth curves for the two-season guayule crop. This is followed by the ET fractions table, which specifies water uptake per layer as a function of root depth. The bimodal guayule evapotranspiration curves are calculated with the WINDS model, and simulated moisture contents are compared to NMM water contents in layers.

3.1. Plant Height and Fractional Canopy Cover Curves for Two-Season Guayule

Segmented plant growth and canopy cover curves were developed for guayule (Figure 3). The plant height curve was based on weekly plant height measurements (Figure 3). The canopy cover curve (f_c) was based on weekly drone RGB measurements (Figure 3). Canopy cover for guayule has three stages: initial (I), development (D) and endseason (E). The simulated f_c and plant height curves are used for the calculation of the evaporation coefficient (K_e). Unlike most crops which have exponential canopy cover curves, the guayule canopy cover increases linearly. The canopy cover has a longer development phase (D) than root depth and plant height. There was complete canopy cover (100% f_c) by the end of the first growing season (180 days). A linear regression equation that represents canopy cover for guayule from RGB measurements was developed by Elshikha et al. [40].

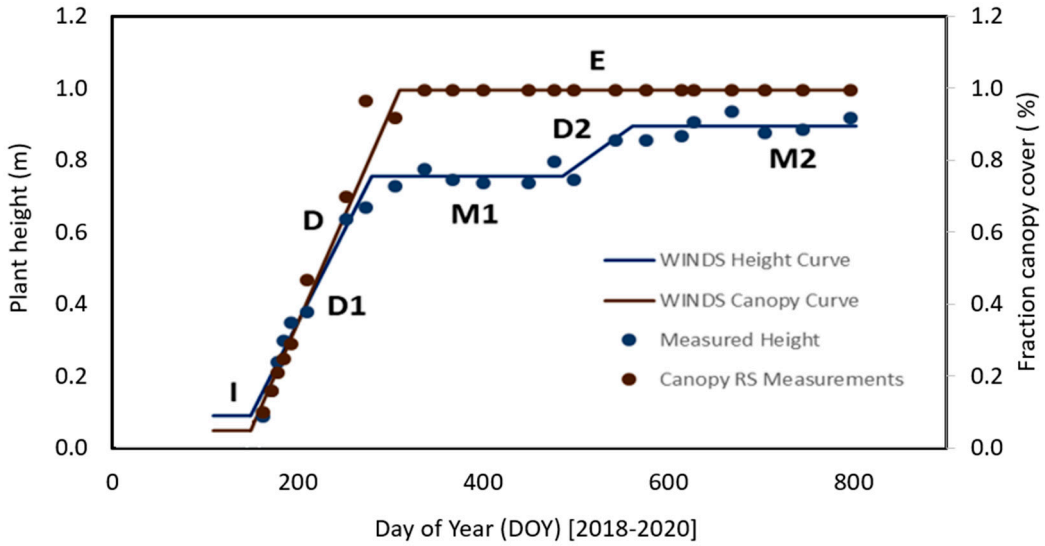

Figure 3. Plant growth curves for crop height and canopy cover (Fc %) for the F100 average treatment. The solid lines are the estimated WINDS height and canopy curves used in the model. The points are the manual plant height measurements and the remote sensing (RS) measurements (RGB (red green blue)). Fc [I = Initial, D = Development, E = Endseason]: Crop Height [I = Initial, D1 = Development year one, M1 = Midseason year one, D2 = Development year two, M2 = Midseason year two]. Day of Year (DOY) refers to days after 1 January 2018.

Plant height and root growth curves have similar two-year growth curves, which consist of an initial stage (I), and two development (D1 & D2) and midseason (M1 & M2) stages (years 1 and 2). Plant height started at 0.10 m at the initial stage and then increased steadily during the first development stage (D1) until it reached a height of 0.73 m by November of 2018. It then remained constant during the first-year midseason (M1) stage during fall and winter seasons. Growth resumed (D2) in March of 2019. It then remained constant after July 2020 (M2). The M1 and M2 plant heights were 0.71 and 0.90, respectively. Specific data for all plant growth and K_{cb} curves are available in Supplemental data in the "Guayule WINDS furrow input" workbook, "Plantings" worksheet.

3.2. Root Growth Curve and Evaporation Fractions per Layer

Guayule has a two-phase root growth pattern (Figure 4). The growth curve was based on observed soil moisture depletion patterns. Roots grew to 1.55 m depth during the first growing season (D1). Root depth remained constant during the winter dormancy period (M1). During the second development phase (D2), roots grew from 1.55 to 2.00 m, which was the lower limit of soil measurements from the NMM. Roots might have grown beyond 2.00 m; however, there was minimal soil water extraction in the lower layers so neglecting root uptake below 2.00 m had minimal effect on the overall simulation. This might not be the case in deficit treatments where roots might pull more water from lower layers.

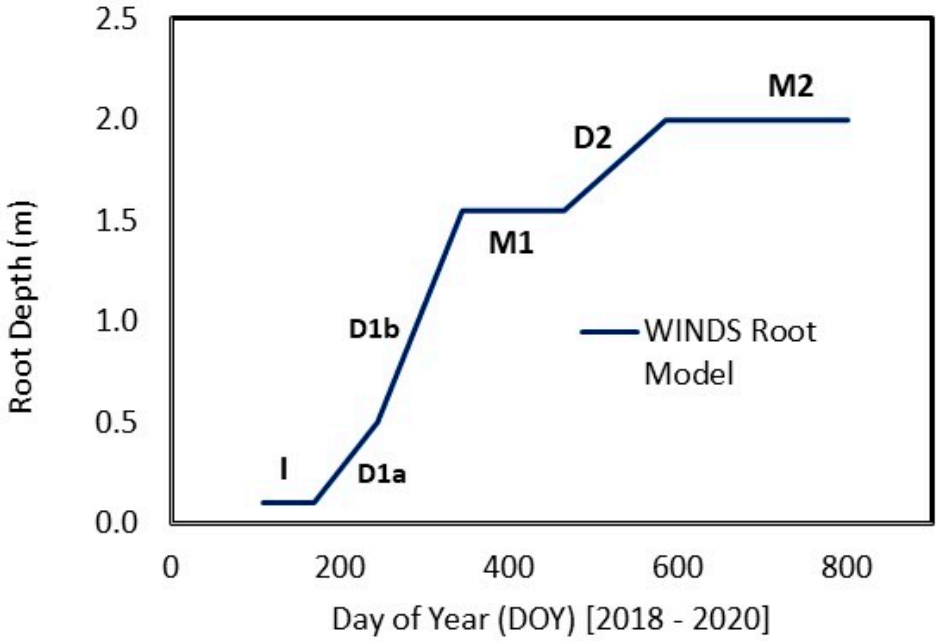

Figure 4. Root growth curves for the F100 average treatment. I = Initial growth stage. D1a = year one development stage part one, D1b = year one development stage part two, M1 = year one midseason stage, D2 = year two development stage, M2 = year two midseason stage. Day of Year (DOY) refers to days after 1 January 2018.

Correlation between the WINDS model soil moisture curves and NMM readings during D1 for the middle layers required a change in slope in root growth during D1. This created two separate D1 development periods (D1a and D1b). During D1a, root depth increased from 0.10 to 0.50 m during the first 75 days (5 mm d^{-1}). During the second part of the first development stage (D1b), root growth rate increased, increasing from 0.50 m to 1.55 m during the next 100 days (10 mm d^{-1}). During the development (D2) phase in year two, depth increased from 1.55 to 2.00 m in 120 days (4 mm d^{-1}).

The ET fractions table (Table 1) assigns fractions of transpiration to layers as a function of root depth. As with root growth, the parameterization of layers for each root growth depth (columns) was based on comparison of the WINDS simulation to observed soil moisture depletion patterns. Most of the transpiration was allocated to the two layers below the evaporation layer (layers 6 and 7). Higher ET fractions in upper layers corresponded with greater fluctuations of water content in the WINDS simulation and in the NMM readings.

Table 1. ET Fraction table for F100 (flood) treatment for different phases of the growing season. Left column is bottom depth of layers. Fractions represent the fraction of total crop transpiration from each layer.

Depth of Layer	Root Penetration Level						
	Layer 7	Layer 6	Layer 5	Layer 4	Layer 3	Layer 2	Layer 1
	Fraction of Transpiration Per Layer						
Evap layer (0–0.11 m)	0.5	0.05	0.05	0.05	0.05	0.05	0.05
Layer 7 (0.11–0.3 m)	0.5	0.49	0.48	0.46	0.42	0.34	0.3
Layer 6 (0.3–0.6 m)	0	0.46	0.43	0.4	0.36	0.34	0.3
Layer 5 (0.6–0.9 m)	0	0	0.04	0.06	0.07	0.09	0.13
Layer 4 (0.9–1.2 m)	0	0	0	0.04	0.05	0.06	0.06
Layer 3 (1.2–1.5 m)	0	0	0	0	0.05	0.0	0.06
Layer 2 (1.5–1.8 m)	0	0	0	0	0	0.06	0.06
Layer 1 (1.8–2.1 m)	0	0	0	0	0	0	0.04

3.3. Basal Crop Coefficient (K_{cb}) Curve

Table 2 lists the K_{cb} stages for guayule. Weekly K_{cb} crop coefficient values were calculated from NDVI values provided by El Shikha et al. (2022). The remote sensing NDVI-K_{cb} relationship was calibrated with data from the same experiment. Then, the segmented K_{cb} curve used in the WINDS model was estimated based on the weekly K_{cb} values (Figure 5).

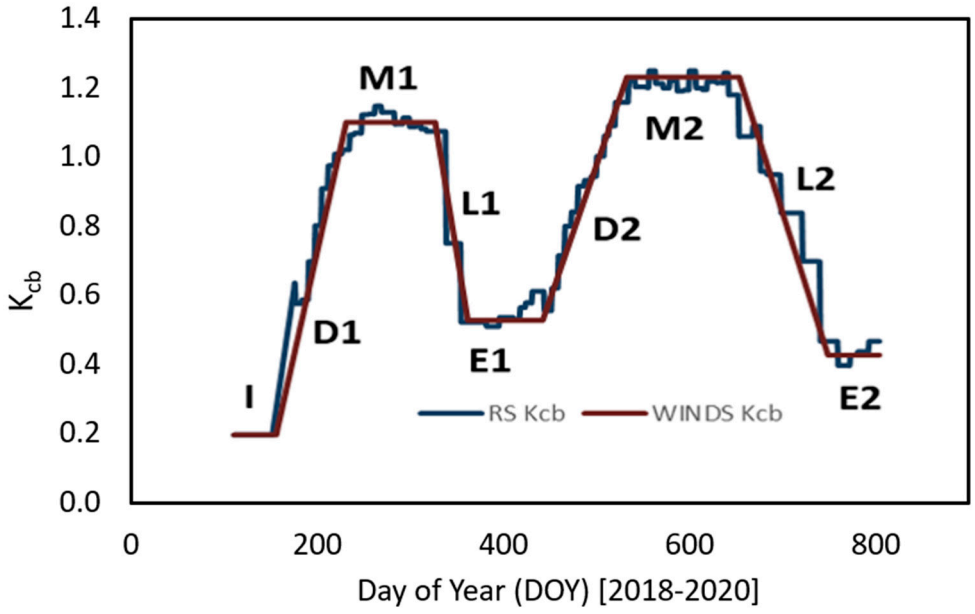

Figure 5. The basal crop coefficient from remote sensing (RS K_{cb}) and WINDS (WINDS K_{cb}) for the guayule flood irrigation treatment. Day of Year (DOY) refers to days after 1 January 2018.

The two seasons had similar development, midseason, and endseason growth periods for this two-year crop (Table 1). The second-year growth stages (D2, M2, L2, E2) had periods that were 1.5 to 2.0 times longer than the first-year growth stages (D1, M1, L1, E1). The first development period, D1, lasted from June to August of 2018. The second season development (D2) went from March to June of 2019. This analysis is based on the typical planting date in April of the first year, but the crop resumes growth from March of the second year; however, commercial guayule production might incorporate different planting and harvest dates due to the possible need to deliver a constant feedstock to the production plant. The K_{cb} for the second summer, M2, was 1.23, which was larger than

the first summer, M1, K_{cb} value of 1.14. This segmented K_{cb} curve resulted in accurate simulation of soil moisture in layers.

Table 2. Basal crop coefficient with nine growth stages of two-season guayule. Day of Year (DOY) refers to days after 1 January 2018.

Name of Growth Stage	DOY Periods	K_{cb} Value(s)	Duration (Days)	Calendar Date Periods
Initial	110–155	0.2	45	April–June 2018
Year One Development (D1)	156–230	0.2–1.1	75	June–August 2018
Year One Midseason (M1)	231–325	1.1	95	August–November 2018
Year One Lateseason (L1)	326–360	1.1–0.53	35	November–December 2018
Year One Endseason (E1)	361–440	0.53	80	January–March 2019
Year Two Development (D2)	441–530	0.53–1.23	90	March–June 2019
Year Two Midseason (M2)	531–650	1.23	120	June–October 2019
Year Two Lateseason (L2)	651–745	1.23–0.45	95	October 2019–January 2020
Year Two Endseason (E2)	746–800	0.45	55	January–March 2020

Although the durations of second year growth stages are larger than the first year, the shapes of the curves are the same. In general, the linear regression equations relating K_{cb} values to NDVI readings (El-Shikha et al., 2021) led to accurate WINDS model simulations. These equations are shown in Figure 6. They represent the development year 1 (D1) and year 2 (D2) growth stages as well as the lateseason year 1 (L1). The NDVI readings taken during these periods represent the range of K_{cb} values throughout the experiment. Most of these K_{cb} numbers take place during the development and lateseason growth stages. The midseason and endseason periods had constant K_{cb} values and thus were not correlated with NDVI.

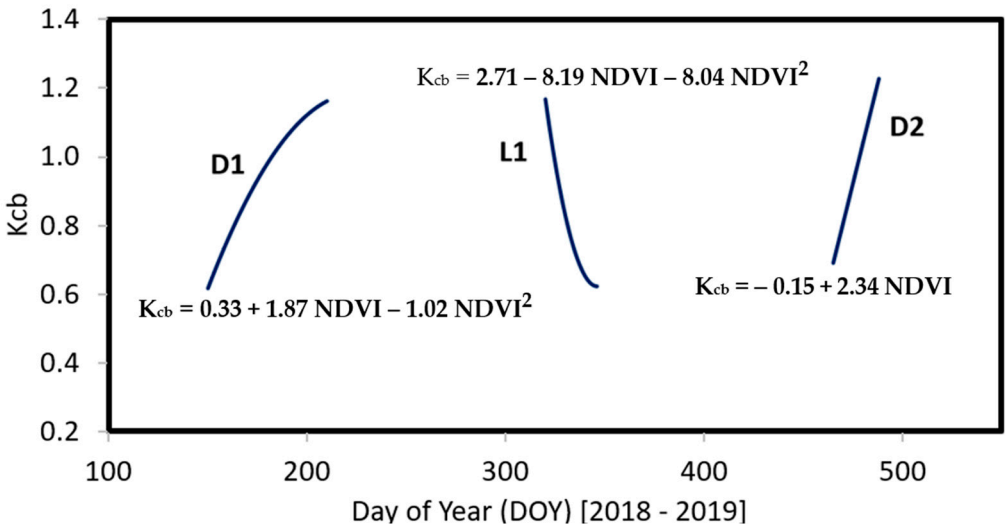

Figure 6. Calibrated basal K_{cb} curves and equations for the development phase of year 1 (D1) and year 2 (D2) as well as the first lateseason (L1) phase, represented as functions of measured NDVI during the time periods (DOY) during 2018–2019. Day of Year (DOY) refers to days after 1 January 2018.

3.4. Evapotranspiration and Irrigation

As a two-season crop, guayule has a bimodal growth and evapotranspiration cycle. Figure 7 shows the reference ET_o, from the weather station, and the WINDS simulation of the two cycles of evaporation, transpiration and crop ET_c. Evaporation was the major component of evapotranspiration in the first several months (Figure 7) and was a function of surface wetting cycles. Thereafter, ET_c was mainly transpiration. During the first winter to mid-summer of the second year, ET_c fell below ET_o. During the second summer, ET_c

fluctuated above and below ET_o, depending on irrigation timing. The ET_c rose above ET_o during the second summer, rising to 13 to 16 mm/day. Thus, the crop coefficient rose to 1.3. Crop ET_c also fell below ET_o during the second winter.

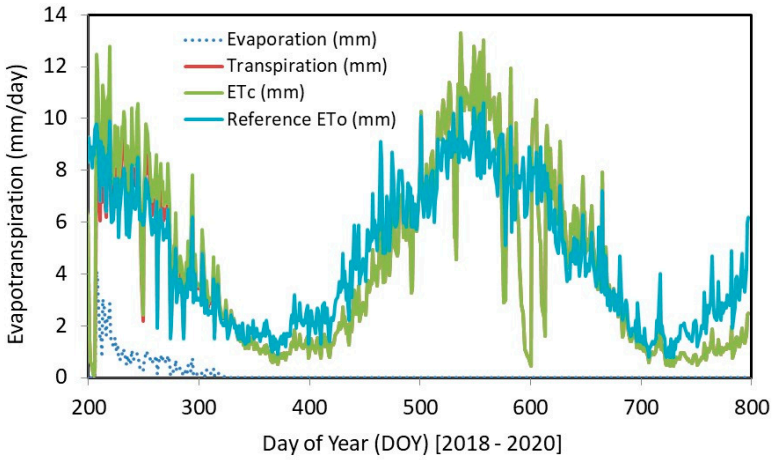

Figure 7. Reference evapotranspiration, crop ET_c, evaporation, and transpiration for the F100 (flood irrigated with 100% replacement of soil water deficit) treatment where Day of Year (DOY) refers to days after 1 January 2018.

Figure 8 shows observed rainfall and irrigation depths. Based on these inputs, the WINDS model calculated daily (Figure 8). Leaching was significant during crop establishment with sprinkler irrigation. There was almost no leaching after crop establishment because the irrigation schedule was based on the level of depletion below field capacity.

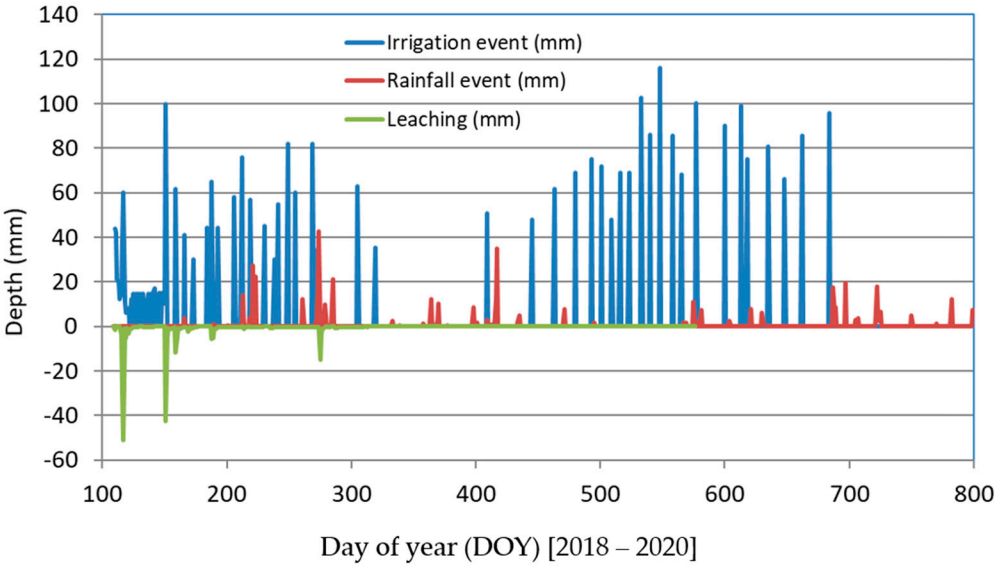

Figure 8. Rainfall, irrigation and leaching (deep percolation below the root zone) events for the F100 irrigation treatment.

After the establishment period, irrigation events were 1 to 2 weeks apart. They were larger and less frequent during the second year because of a deeper root zone. Irrigation events were generally in the range of 70 to 90 mm. Irrigation was cut off during winters. Precipitation was minimal in comparison to irrigation. There were large rainfall events during the first fall seasons, but only a few precipitation events were greater than 10 mm during the second year and a half.

3.5. WINDS Simulation of Soil Moisture

In the WINDS model, field capacity (FC) and permanent wilting point (WP) were based on observed neutron probe readings of soil moisture in layers. Neutron probe readings were collected one to two days after irrigation events, which allowed time for drainage to field capacity prior to the readings in sandy loam soils. Thus, FC was the maximum neutron probe moisture content in each layer. Guayule removes water almost to the permanent wilting point during winter dormancy. Thus, the low neutron probe moisture content in each layer was assumed to be WP. An example of FC and WP levels is shown in Figure 9 for the sixth layer. The upper black line in the figures represents the FC while the lower line is the WP. In this case, layer 6 had an FC of 25% and a WP of 14%. Table 1 shows the average FC and WP in all layers. The field was over irrigated during germination and crop establishment, so the initial water content in all layers for the simulation was field capacity.

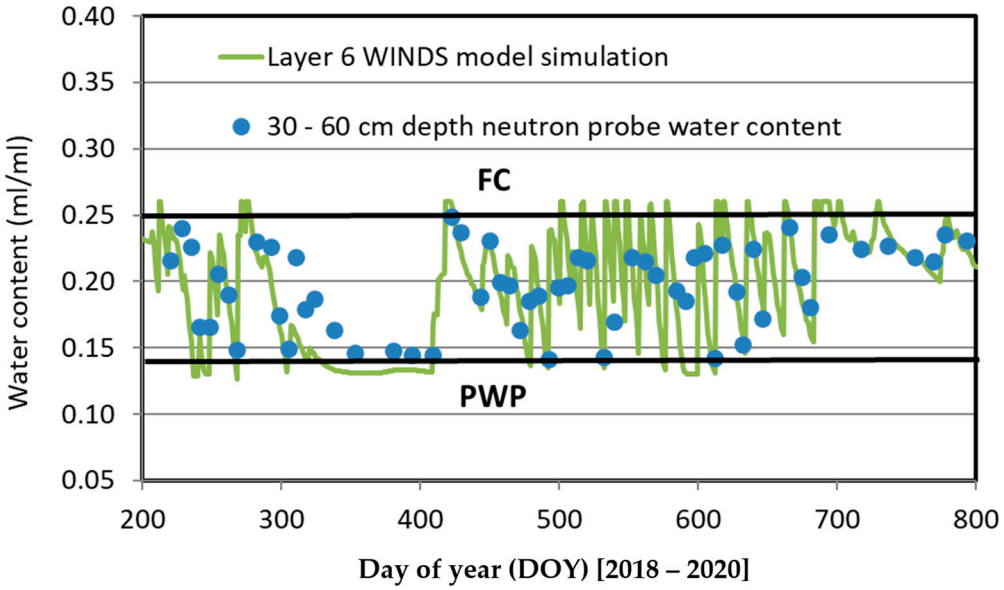

Figure 9. Assignment of Field Capacity (FC) and Permanent Wilting Point (WP) in layer 6 (30–60 cm depth) based on observed maximum and minimum NMM water content readings, respectively.

During days with no infiltration (irrigation or precipitation) events, the WINDS model uses Richards equation to calculate water flux between layers based on energy gradients. The Richards equation uses the Van Genuchten-Mualem (VG-M) relationships between water content, matric potential, and hydraulic conductivity. The VG m coefficients were assigned with the Rosetta model [47] based on sand, silt, and clay percentages in the upper 30 cm. They were close to the default values for sandy loam soils. On days with infiltration events (irrigation or precipitation), the tipping bucket model distributes downward moving water based on field capacity and antecedent depletion. Because almost all water flux in sandy loam soils takes place on the irrigation day, the WINDS model is insensitive to the Richards equation and VG m parameters in the sandy loam soils at Maricopa Agricultural Center [38]. While upward movement from lower layers might have a low rate of water flux, this was a minor part of the total water balance. Thus, the most important parameters in the simulation were FC and PWP (Table 3).

After calibration of soil, root, and crop parameters, the WINDS model was closely correlated with the observed NMM water content readings during the entire experiment (August 2018 to March 2020). Figure 10 shows WINDS model soil moisture simulations and NMM water content readings for the soil profile, consisting of seven soil layers plus an evaporation layer. The NMM readings in Figure 10 represent averages of the five of the six

access tube locations in the flood irrigation treatment. One access tube was left out of the average because it had different soil characteristics in the lower layers.

Table 3. Field capacity (FC) and permanent wilting point (PWP), and initial water content (IW), average for the flood treatment (F100).

Layer Number	Lower Boundary (m)	IW (%)	FC (%)	WP (%)
8	0.1	27.5	27.5	10.0
7	0.3	27.5	27.5	10.0
6	0.6	25.0	25.0	14.0
5	0.9	28.0	28.0	17.0
4	1.2	28.0	28.0	17.0
3	1.5	22.5	22.5	14.0
2	1.8	20.0	20.0	13.5
1	2.1	20.5	20.5	15.0

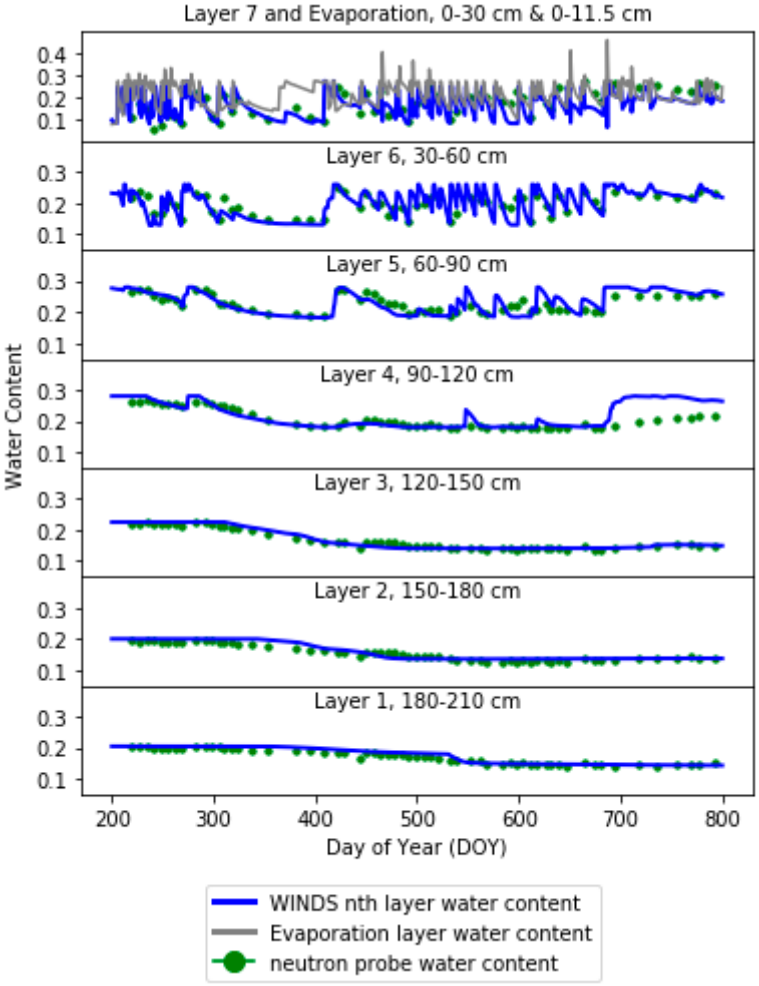

Figure 10. The F100 (flood irrigated) average water content curve simulations and neutron probe (NMM) measurements for all soil layers and evaporation layer.

There were frequent and large soil moisture cycles in the upper soil layers (layers 6 and 7). Moisture cycles decreased in frequency and intensity with depth because most transpiration takes place in the upper layers. These levels of transpiration are reflected in the high values in the upper rows of the ET Fraction worksheet (Table 2). The evaporation layer, gray line in upper figure, is not represented by neutron probe measurements, which do not accurately measure evaporation layer water content.

The middle layers, which are at the boundary of infiltration, had inconsistent behavior; thus, characterizing the responses of the middle layers to irrigation events was challenging. Layer four did not respond to any irrigation events in the observed moisture contents but had two responses in the *WINDS* model; thus, there was a discrepancy between the *WINDS* model and the observed NMM readings at the end of the experiment in layer 4, which demonstrates the difficulty of simulating layers at the boundary of infiltration. The period with the least accurate simulation was the last 150 days.

Neither the *WINDS* model, nor the observed data showed any responses to infiltration events in the lower three layers. After soil moisture was brought to FC in the entire soil profile during establishment, the lower layers gradually decreased in soil moisture over the two years. The lowest layers were the last to reach minimum soil moisture. To simulate this pattern in the *WINDS* model, roots reached the lowest layers during the second year; however, the fraction of total ET from these layers (Table 1) remained low.

3.6. WINDS Response to Soil Variability

This section evaluates the ability of the WINDS model to simulate water contents for varying soil properties in replicates. The six NMM readings along with the average WINDS model soil moisture simulations are shown in Figures A1–A7 in the Appendix A. The different replicates (R1–R6) exhibit similar trends in moisture content although they have different values of FC and WP. The previous adjustments of crop, root growth and uptake parameters for the average of the replicates resulted in accurate simulations in replicates with changes in WINDS FC and WP values for each replicate. One replicate (R5, Figures A3–A5) had much lower soil moisture content readings in layers three to five than the other replicates. Thus, the replicate was not included in the average, nor did the calibrated WINDS model accurate simulate these layers. The lower water contents might have been due to a sandy lens or another discontinuity. In general, the upper layers had similar soil properties between access tubes, which is probably due to long-term cultivation practices and associated soil mixing.

The fact that adjustment of parameters for the average resulted in accurate simulations of the individual replicates implies that once the *WINDS* model ET fraction and crop parameters are adjusted for a certain crop, soil type, and climate, it can be transferred to other fields with similar but not the same soil characteristics.

The correlation between all *WINDS* model soil moisture curves and the NMM readings was tested statistically with a root mean square error (RMSE) analysis. The results of this analysis are shown in Table 4. The majority of the RMSE values were well below 5%, usually in the range of 1–3% (Table 4). Only layer seven had RMSEs larger than 5% along with layer one for the R2 replicate. They were high for layer seven because it includes the evaporation layer which behaves differently than the layer below it.

Table 4. Volumetric water content root mean square error for different soil layers (1–7). Where layer seven is the layer below the evaporation layer in the WINDS model, but the NMM reading represents both layers. The values represent the percent water content difference between the WINDS model and the measured water content. Each replicate refers to an access tube.

Layer	F100 R1 RMSE (% WC)	F100 R2 RMSE (% WC)	F100 R3 RMSE (% WC)	F100 R4 RMSE (% WC)	F100 R5 RMSE (% WC)	F100 R6 RMSE (% WC)	F100 AVE RMSE (% WC)
7	6.93	7.83	6.95	5.88	6.74	6.84	6.20
6	2.54	3.77	2.40	2.65	2.82	2.40	2.51
5	2.40	2.46	2.18	2.33	3.49	2.68	2.19
4	2.26	2.41	2.28	2.39	2.80	2.32	2.39
3	1.66	2.55	2.40	2.89	3.31	1.50	0.75
2	1.45	1.42	0.90	0.97	2.32	2.09	1.00
1	1.50	5.37	1.19	1.14	1.63	1.11	0.73

4. Discussion

This research evaluated the ability of the WINDS model to simulate a guayule crop in sandy loam soils in central Arizona. It developed guayule crop and root growth curves that enable WINDS model simulation of guayule irrigation, crop water use, and moisture content in research experiments and production agriculture.

Elshikha et al. [40] developed equations for plant cover and basal crop coefficient (K_{cb}) based on multispectral and RGB indices, as well as measured irrigation application and water use. This research built on the results of [40] and developed segmented canopy cover and basal crop coefficient (K_{cb}) curves (Figures 3 and 5) for the entire two-year growth cycle. The segmented curves were used as input data for the WINDS model.

By comparing NMM data and WINDS simulations, a six-phase segmented root growth curve was developed for the two-season guayule crop (Figure 4). The same comparisons were used to develop the ET fractions table (Table 1), specifying fractions of transpiration removed from each soil layer as a function of total root depth.

For the average and in each replicate, field capacity (FC) and permanent wilting point (WP) were specified in each layer (Table 3) based on observed maximum and minimum NMM moisture contents.

With the average FC and WP for each layer, the WINDS model accurately simulated of soil moisture content changes for the average NMM moisture contents over the two-year growth cycle (Figure 10). The RMSE was in the range of 1% to 3% moisture content for all layers except the evaporation layer. There was no moisture measurement in the evaporation layer. Next, the WINDS model was evaluated for its ability to simulate moisture content in the replicates (Appendix A Figures A1–A6), which had slightly different FC and PWP values. Again, the RMSE values were in the range of 1% to 3% moisture content. Thus, once the WINDS model was parameterized for one soil, it can accurately simulate moisture content in similar soils with slightly varying FC and WP values.

We are not aware of other daily time-step models that can provide an accurate representation of water contents within layers throughout the entire soil profile. The ultimate goal is to use WINDS in tandem with soil moisture sensors and remote sensing in order to optimize irrigation, which requires accurate simulation of water content in layers.

The online WINDS app (https://viz.datascience.arizona.edu/WINDS/, 10 September 2023) is designed for irrigation management of guayule and other crops in the arid southwestern United States. The posted app allows selection of the many SBAR experiments and treatments, as well as past experiments in cotton [38]. The online app replicates the calculations shown in Figure 10. It also allows the selection of any layer for both WINDS simulation and neutron probe readings. In Figure A8 (Appendix A), the F100 Ave treatment was selected, as well as the Layer 6 WINDS simulation, season view. The neutron probe box was checked to add the neutron probe readings to the graph. The user can select any or all WINDS simulation layers as well as any or all neutron probe readings. In this case, only layer 6 WINDS simulation and neutron probe readings are shown in Figure A8. The user can select Day of year, days after planting, or date as the time scale.

The WINDS model also has a daily view mode that shows water content as a function of depth in the soil profile and estimates the date of the next irrigation based on the WINDS model simulation (Figures A8 and A9), This view shows the height of the plant and the percent canopy cover by the height and proximity of the plants. It also shows the depth of the root zone. The scroll bar allows the user to scroll to any day during the growing season. The soil profile on the left is color-coded with the range below WP in red, between WP and MAD in yellow, between MAD and FC in green, and between FC and saturation in blue. The irrigation scheduler on the right uses the same colors to represent water content in the entire soil profile. Blue represents the range from FC to saturation. Green represents the range from MAD to FC. Yellow represents the range from WP to MAD, and red represents the range from WP to MAD. The scroll bar allows selection of any day after planting. Figure A9 shows the day after planting 131, which is during the first summer when the roots had only extended into layer 6. The irrigation scheduler sums the water depletion

in the layers within the root zone. The fraction depletion in each layer is the difference between field capacity and water content. The total depletion for the root zone is the sum of (fraction depletion) (layer depth) for all layers in the root zone. This total depletion is reported in the graphic on the right side of the irrigation scheduler (Figure A10). The model also calculates the expected ET for the subsequent days and recommends the number of days before the next irrigation. Figure A10 shows day 549, which is during the second winter. At this time the crop is semi dormant and has extracted the water in almost all layers to the WP. The plant canopy is completely closed and plants are at their full height.

5. Conclusions

Based on remote sensing and water balance observation from [40], the WINDS model was calibrated for a two-year guayule crop by developing the following two-year segmented curves.

1. Two-year segmented basal crop coefficient curve
2. Canopy cover curve
3. Two-year crop height curve
4. Two-year six-phase segmented root growth curve

Based on comparison of WINDS simulations with NMM water contents, root activity in layers was delineated, as tabulated in the ET fractions table, which specifies transpiration fractions from soil layers as a function of root depth.

With crop and root curves, as well as reference ET from the AZMET weather station, the WINDS model accurately simulated the average soil moisture content of furrow (flood) irrigated guayule during the two-year (2018–2020) guayule growth cycle for the average of five replicate NMM water contents in layers. The RMSE ranged from 1% to 3% water content for all layers below the evaporation layer. The individual NMM access tubes had varying FC and WP values. Nevertheless, the WINDS model accurately simulated the individual NMM water content observations, with adjusted FC and WP values, also with RMSE in the range of 1% to 3%.

Author Contributions: Conceptualization, P.M.W., D.J.H., D.E.M.E. and K.L.O.; methodology, P.M.W., D.J.H., D.E.M.E. and K.L.O.; software, P.M.W., R.S.L. and M.E.K.; validation, M.E.K.; formal analysis, M.E.K.; investigation, M.E.K., D.E.M.E. and P.M.W.; resources, G.W.W.; data curation, M.E.K.; writing—original draft preparation, M.E.K.; writing—review and editing, P.M.W., D.E.M.E. and G.W.W.; visualization, M.E.K. and D.E.M.E.; supervision, P.M.W. and D.E.M.E.; project administration, P.M.W. and K.L.O.; funding acquisition, K.L.O. All authors have read and agreed to the published version of the manuscript.

Funding: This project was supported by the Sustainable Bioeconomy for Arid Regions (SBAR), USDA National Institute of Food and Agriculture (NIFA), USA Grant no. 2017-68005-26867.

Data Availability Statement: Data for this research project are available in the Excel spreadsheet WINDS-Cotton-2007.

Conflicts of Interest: The authors declare no conflict of interest.

Appendix A

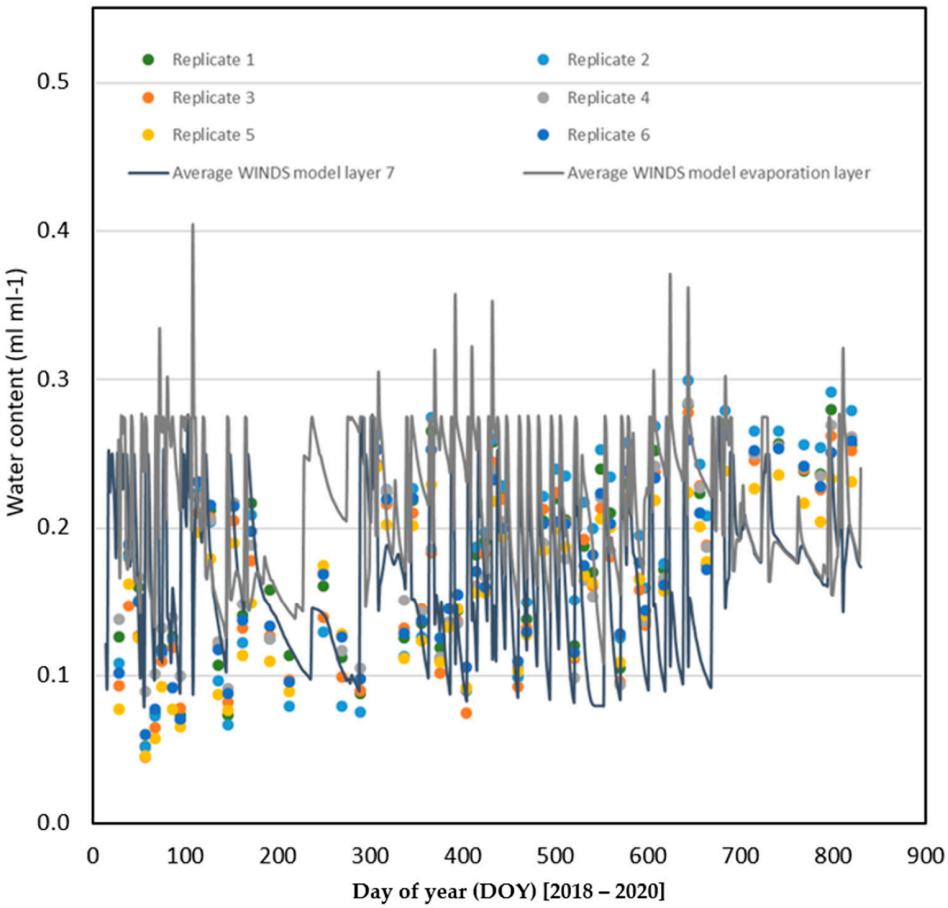

Figure A1. The NMM measurements (0.2 m depth) for the six neutron access tubes in the F100 flood treatment as well as the average WINDS water content curves for layer 7 (0.11 to 0.3 m depth) and the evaporation layer (0 to 0.11 m depth).

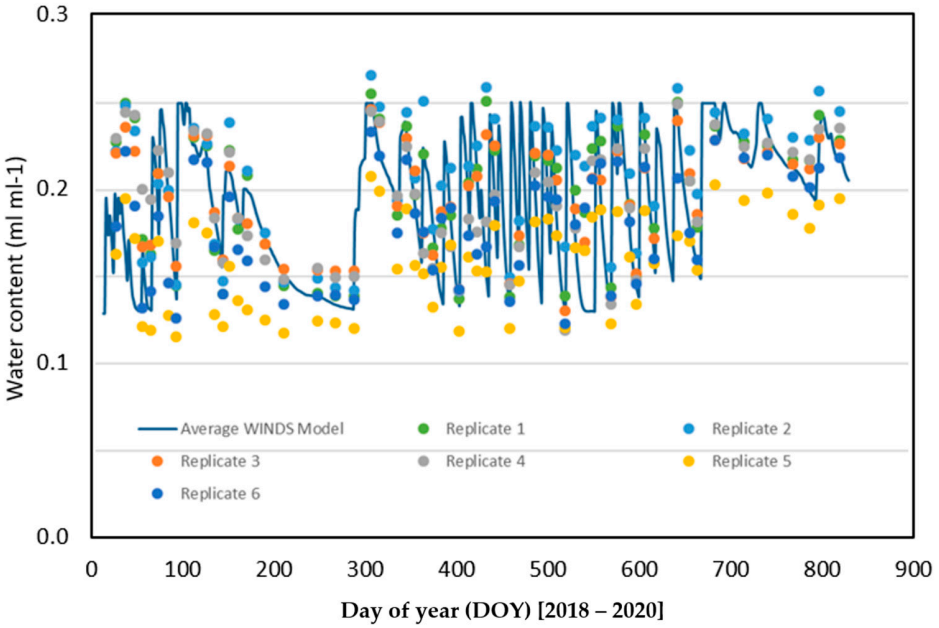

Figure A2. The NMM measurements at 0.45 m depth for the six neutron access tubes in the F100 flood treatment as well as the average WINDS water content curves for layer 6 (0.3 to 0.6 m depth).

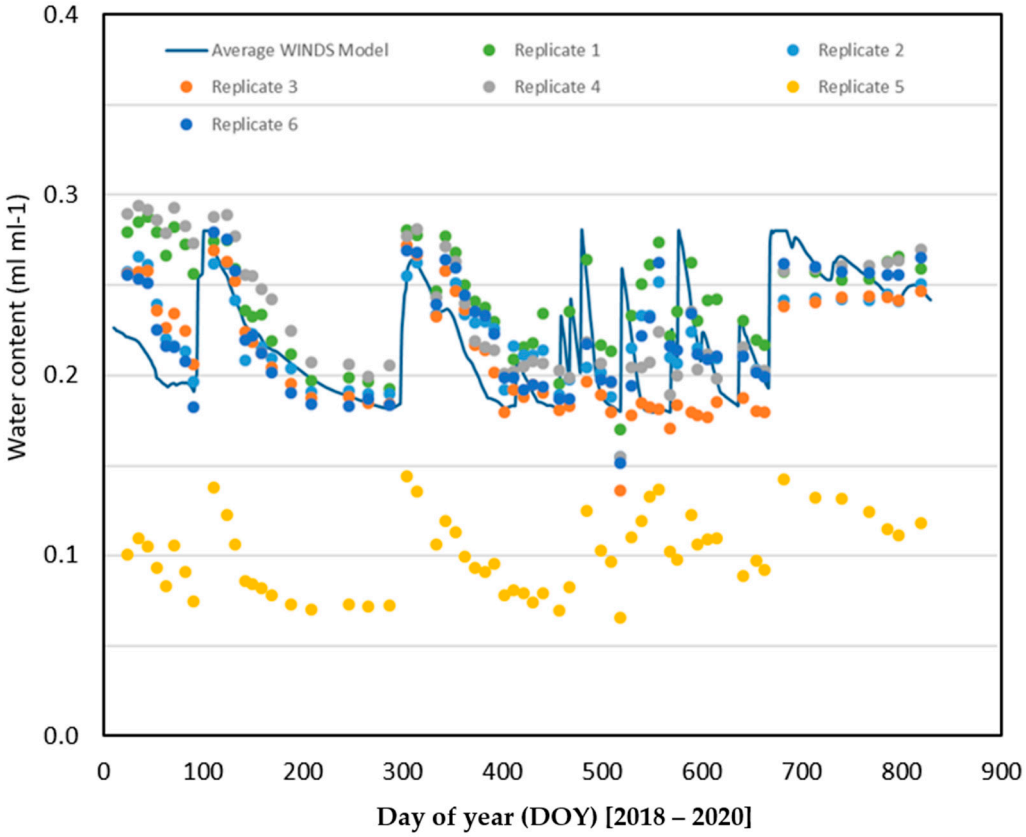

Figure A3. The NMM measurements at 0.75 m depth for the six neutron access tubes in the F100 flood treatment as well as the average WINDS water content curves for layer 5 (0.6 to 0.9 m depth).

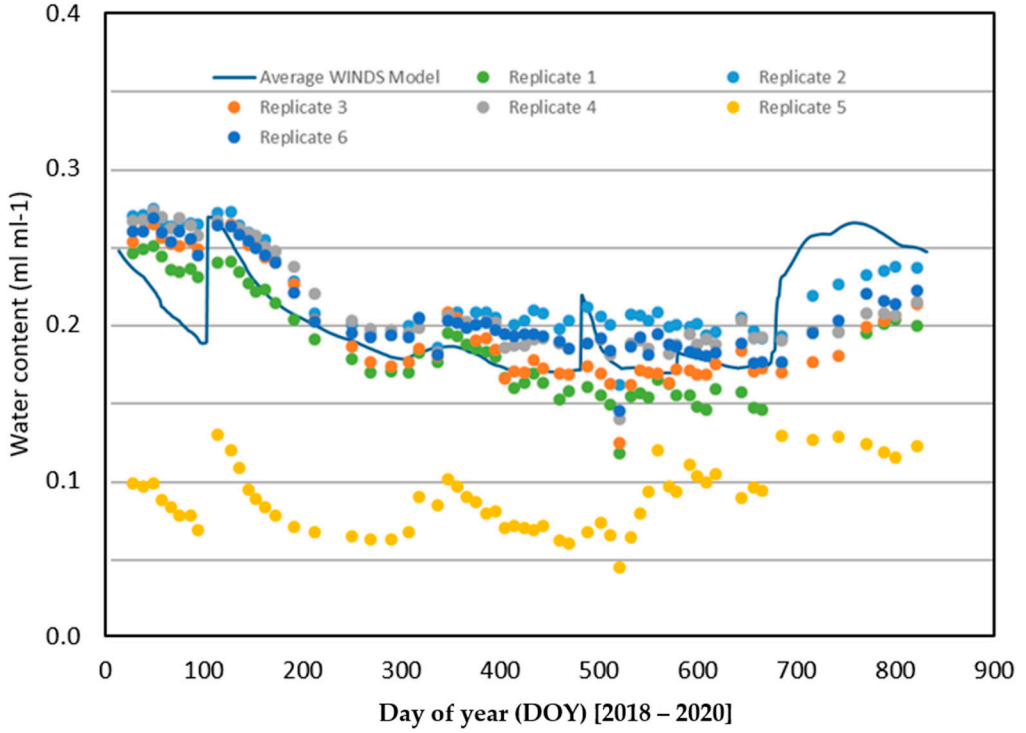

Figure A4. The NMM measurements at 1.05 m depth for the six neutron access tubes in the F100 flood treatment as well as the average WINDS water content curves for layer 4 (0.9 to 1.2 m depth).

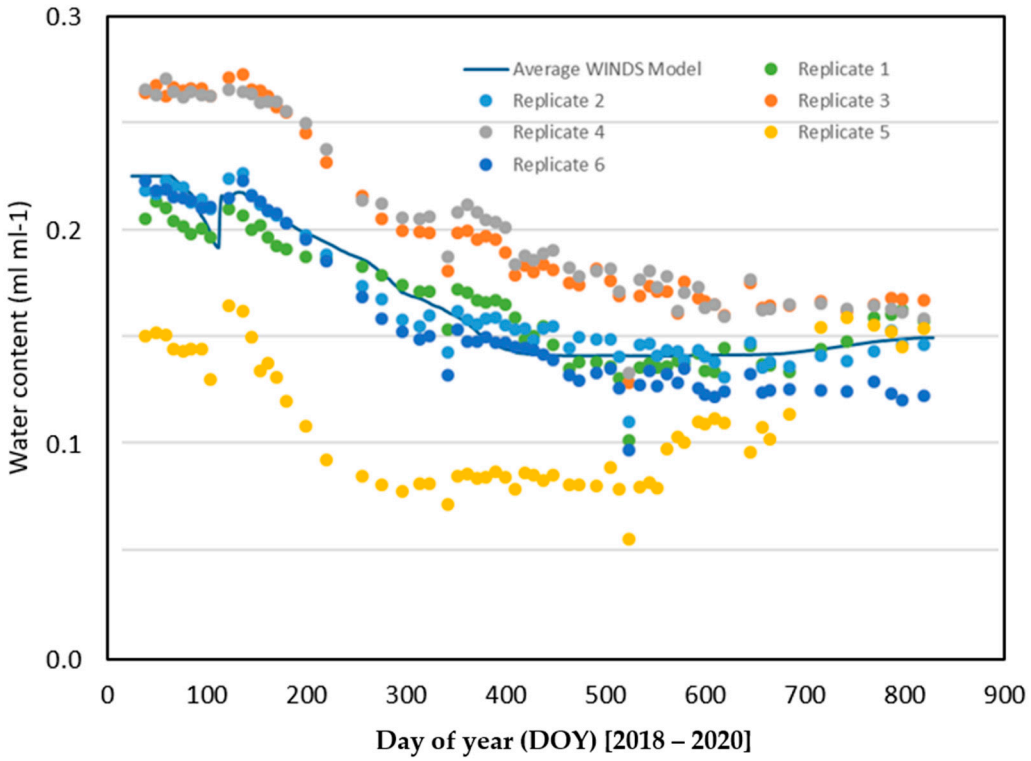

Figure A5. The NMM measurements at 1.35 m depth for the six neutron access tubes in the F100 flood treatment as well as the average WINDS water content curves for layer 3 (1.2 to 1.5 m depth).

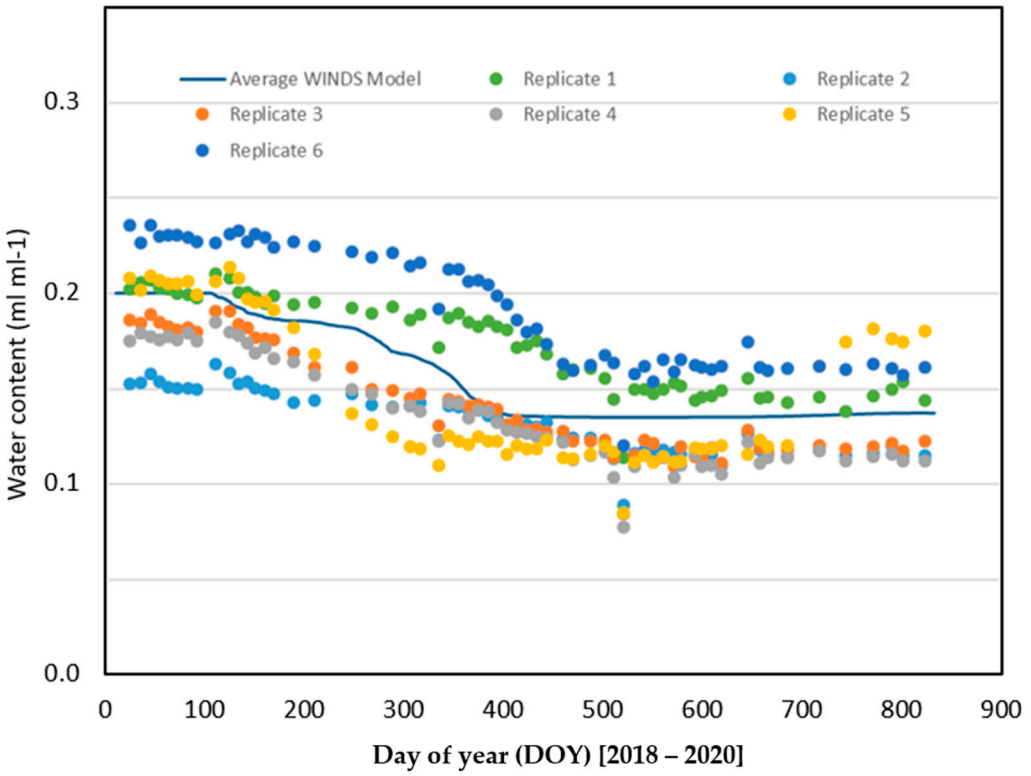

Figure A6. The NMM measurements at 1.65 m depth for the six neutron access tubes in the F100 flood treatment as well as the average WINDS water content curves for layer 2 (1.5 to 1.8 m depth).

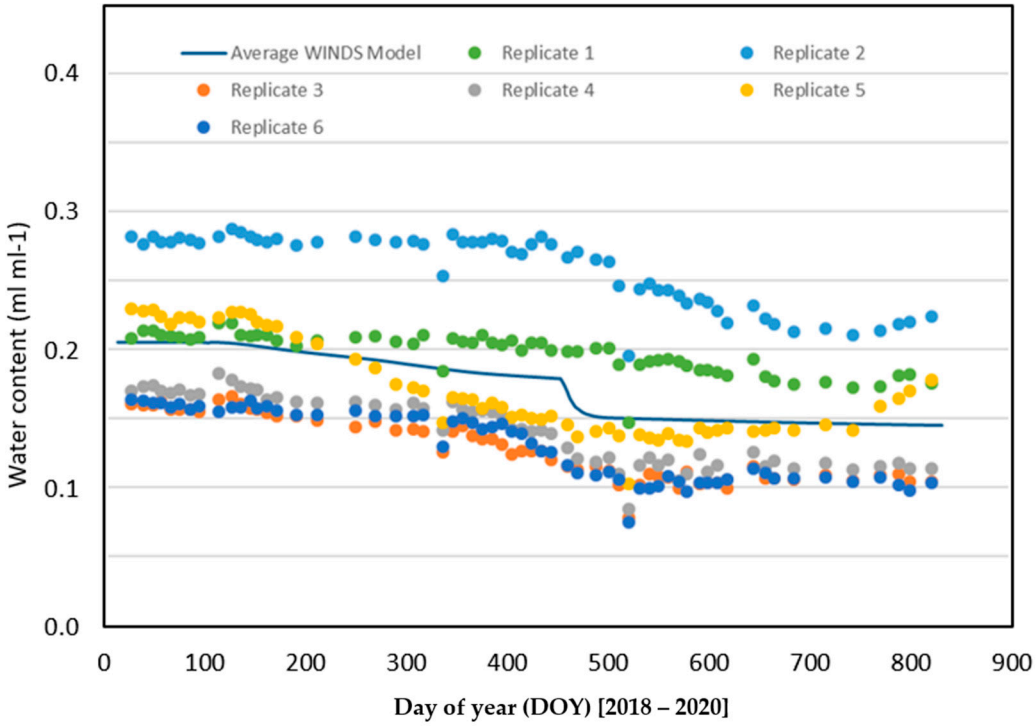

Figure A7. The NMM measurements at 1.95 m depth for the six neutron access tubes in the F100 flood treatment as well as the average WINDS water content curves for layer 1 (1.8 to 2.1 m depth).

Figure A8. The WINDS app simulation of F100 (flood irrigated) average water content and neutron probe readings at 45 cm for layer 6 (0.3 to 0.6 cm depth), season view.

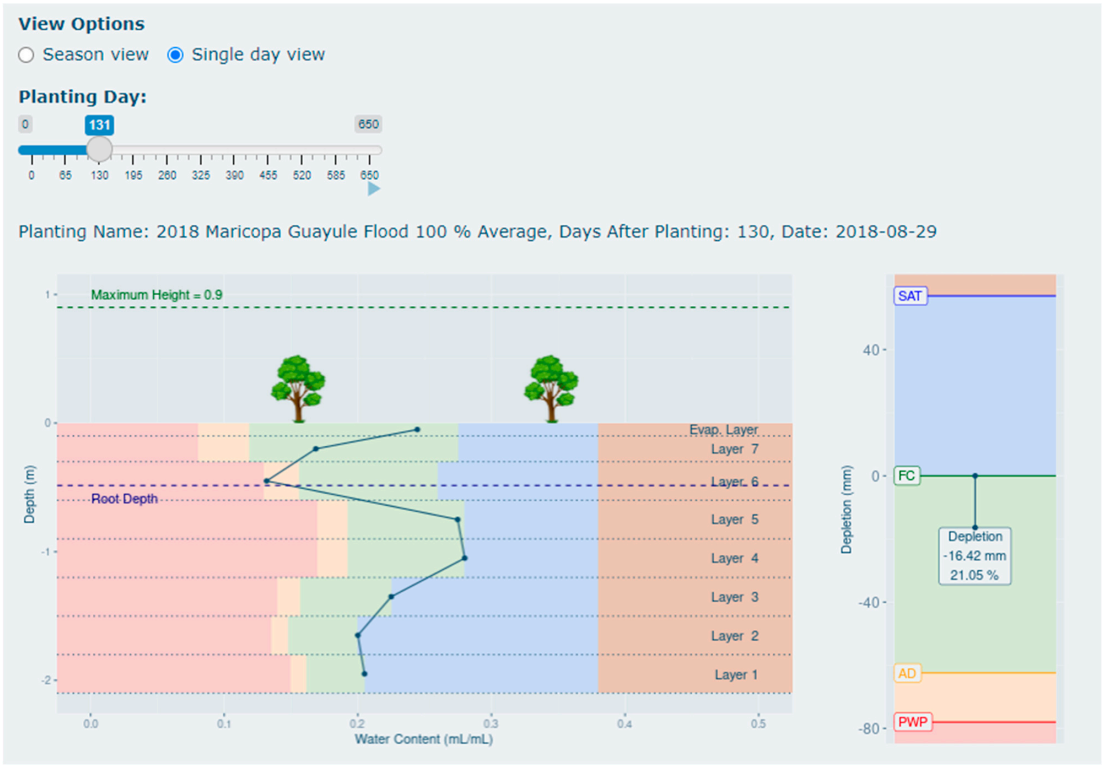

Figure A9. The WINDS app simulation of F100 (flood irrigated) average water content in each layer 131 days after planting, daily view with irrigation scheduler on the right.

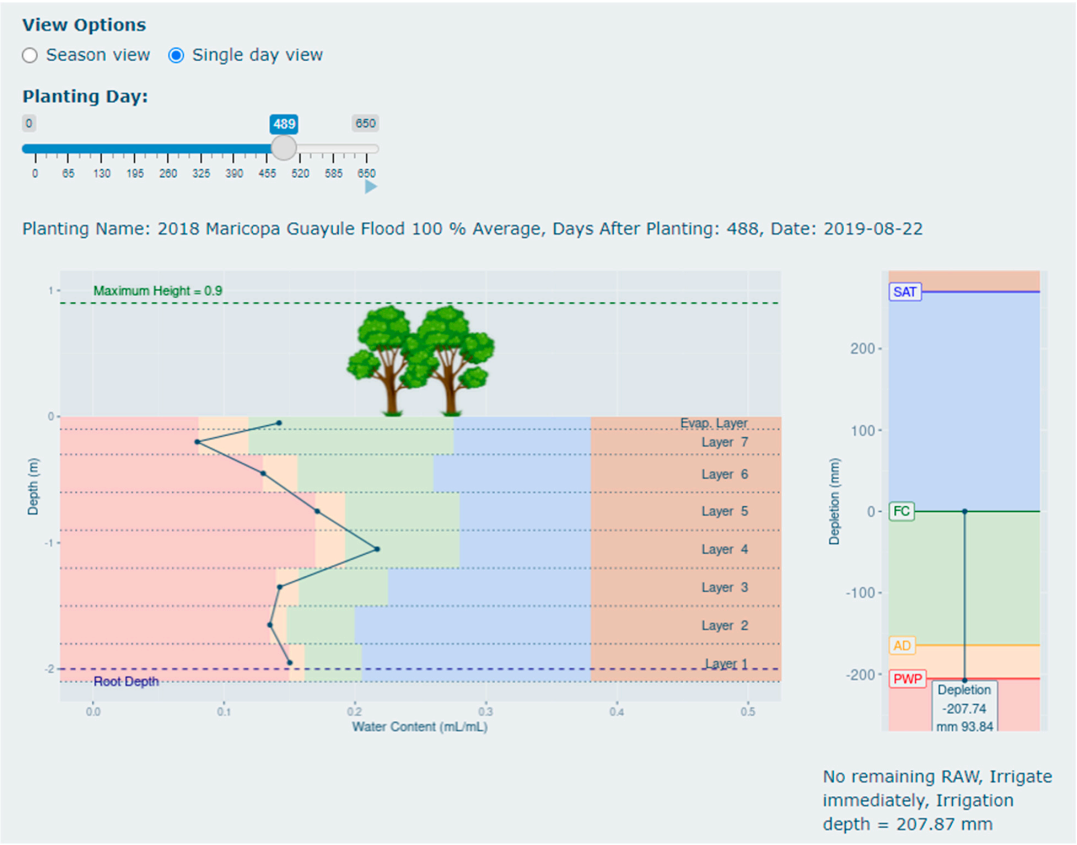

Figure A10. The WINDS app simulation of F100 (flood irrigated) average water content in each layer 489 days after planting, daily view with irrigation scheduler on the right.

References

1. Mpanga, I.K.; Idowu, O.J. A decade of irrigation water use trends in southwestern USA: The role of irrigation technology, best management practices, and outreach education programs. *Agric. Water Manag.* **2021**, *243*, 106438. [CrossRef]
2. Lahmers, T.; Eden, S. *Water and Irrigated Agriculture in Arizona*; Arroyo, University of Arizona Water Resources Research Center: Tucson, AZ, USA, 2018.
3. Rasutis, D.; Soratana, K.; McMahan, C.; Landis, A.E. A sustainability review of domestic rubber from the guayule plant. *Ind. Crops Prod.* **2015**, *70*, 383–394. [CrossRef]
4. Nakayama, F.S. Guayule future development. *Ind. Crops Prod.* **2005**, *22*, 3–13. [CrossRef]
5. Nakayama, F.S.; Bucks, D.A.; Roth, R.I.; Gardner, B.R. Guayule biomass production under irrigation. *Bioresour. Technol.* **1991**, *35*, 173–178. [CrossRef]
6. Coffelt, T.A.; Ray, D.T. Cutting height effects on guayule latex, rubber, and resin yields. *Ind. Crops Prod.* **2010**, *32*, 264–268. [CrossRef]
7. Fangmeier, D.D.; Samani, Z.; Garrot, D., Jr.; Ray, D.T. Water effects on guayule production. *Trans. ASAE* **1985**, *28*, 1947–1950. [CrossRef]
8. Elshikha, D.M.; Wang, G.; Waller, P.M.; Hunsaker, D.J.; Dierig, D.; Thorp, K.R.; Thompson, A.; Katterman, M.E.; Herritt, M.T.; Bautista, E.; et al. Guayule growth and yield responses to deficit irrigation strategies in the U.S. desert. *Agric. Water Manag.* **2023**, *277*, 108093. [CrossRef]
9. Bucks, D.A.; Nakayama, F.S.; French, O.F.; Legard, W.W.; Alexander, W.L. Irrigated guayule-evapotranspiration and plant water stress. *Agric. Water Manag.* **1985**, *10*, 61–79. [CrossRef]
10. Bucks, D.B.; Nakayama, F.S.; French, O.F.; Rasnick, B.A.; Alexander, W.L. Irrigated guayule-plant growth and production. *Agric. Water Manag.* **1985**, *10*, 81–93. [CrossRef]
11. Hunsaker, D.J.; Elshikha, D.M. Surface irrigation management for guayule rubber production in the US desert Southwest. *Agric. Water Manag.* **2017**, *185*, 43–57. [CrossRef]
12. Elshikha, D.M.; Waller, P.M.; Hunsaker, D.J.; Dierig, D.; Wang, G.; Cruz, V.M.V.; Thorp, K.R.; Katterman, M.E.; Bronson, K.F.; Wall, G.W. Growth, water use, and crop coefficients of direct-seeded guayule with furrow and subsurface drip irrigation in Arizona. *Ind. Crops Prod.* **2021**, *170*, 113819. [CrossRef]
13. Car, N.J.; Christen, E.W.; Hornbuckle, J.W.; Moore, G.A. Using a mobile phone Short Messaging Service (SMS) for irrigation scheduling in Australia–Farmers' participation and utility evaluation. *Comput. Electron. Agric.* **2012**, *84*, 132–143. [CrossRef]
14. Pereira, L.S.; Paredes, P.; Jokanovic, N. Soil water balance models for determining crop water and irrigation requirements and irrigation scheduling focusing on the FAO56 method and the dual K_c approach. *Agric. Water Manag.* **2020**, *241*, 106357. [CrossRef]
15. Steduto, P.; Hsiao, T.C.; Raes, D.; Fereres, E. AquaCrop–The FAO crop model to simulate yield response to water: I. Concepts and underlying principles. *J. Agron.* **2009**, *101*, 426–437. [CrossRef]
16. Smith, M. *CROPWAT: A Computer Program for Irrigation Planning and Management (No. 46)*; Food and Agriculture Organization of the United Nations: Rome, Italy, 1992.
17. Rosa, R.D.; Paredes, P.; Rodrigues, G.C.; Alves, I.; Fernando, R.M.; Pereira, L.S.; Allen, R.G. Implementing the dual crop coefficient approach in interactive software. I. Background and computational strategy. *Agric. Water Manag.* **2012**, *103*, 8–24. [CrossRef]
18. Allen, R.G.; Pereira, L.S.; Raes, D.; Smith, M. *Crop Evapotranspiration-Guidelines for Computing Crop Water Requirements-FAO Irrigation and Drainage Paper 56*; Food and Agriculture Organization of the United Nations: Rome, Italy, 1998; p. 300.
19. Pereira, L.S.; Paredes, P.; Lopez-Urrea, R.; Hunsaker, D.J.; Mota, M.; Mohammadi, S.Z. Standard single and basal crop coefficients for vegetable crops, an update of FAO56 crop water requirements approach. *Agric. Water Manag.* **2021**, *243*, 106196. [CrossRef]
20. Pereira, L.S.; Parades, P.; Hunsaker, D.J.; Lopez-Urrea, R.; Mohammadi, S.Z. Standard single and basal crop coefficients for field crops. Updates and advances to the FAO56 crop water requirements method. *Agric. Water Manag.* **2021**, *243*, 106466. [CrossRef]
21. Gallardo, M.; Jackson, L.E.; Schulbach, K.; Synder, R.L.; Thompson, R.B.; Wyland, L.J. Production and water use in lettuces under variable water supply. *Irrig. Sci.* **1996**, *16*, 125–137. [CrossRef]
22. Bryla, D.R.; Trout, T.J.; Ayars, J.E. Weighing lysimeters for developing crop coefficients and efficient irrigation practices for vegetable crops. *HortScience* **2010**, *45*, 1597–1604. [CrossRef]
23. Thorp, K.R.; Hunsaker, D.J.; Bronson, K.F.; Andrade-Sanchez, P.; Barnes, E.M. Cotton irrigation scheduling using a crop growth model and FAO-56 methods: Field and simulation studies. *Trans. ASABE* **2017**, *60*, 2023–2039. [CrossRef]
24. Hunsaker, D.J.; Bronson, K.F. FAO56 crop and water stress coefficients for cotton using subsurface drip irrigation in an arid US climate. *Agric. Water Manag.* **2021**, *252*, 106881. [CrossRef]
25. Hunsaker, D.J.; Barnes, E.M.; Clarke, T.R.; Fitzgerald, G.J.; Pinter, P.J., Jr. Cotton irrigation scheduling using remotely sensed and FAO-56 basal crop coefficients. *Trans. ASAE* **2005**, *48*, 1395–1407. [CrossRef]
26. Hunsaker, D.J.; Fitzgerald, G.J.; French, A.N.; Clarke, T.R.; Ottman, M.J.; Pinter, P.J., Jr. Wheat irrigation management using multispectral crop coefficients: I. Crop evapotranspiration prediction. *Trans. ASABE* **2007**, *50*, 2017–2033. [CrossRef]
27. Johnson, L.F.; Trout, T.J. Satellite NDVI assisted monitoring of vegetable crop evapotranspiration in California's San Joaquin Valley. *Remote Sens.* **2012**, *4*, 439–455. [CrossRef]
28. Bispo, R.C.; Hernandez, F.B.T.; Gonçalves, I.Z.; Neale, C.M.U.; Teixeira, A.H.C. Remote sensing based evapotranspiration modeling for sugarcane in Brazil using a hybrid approach. *Agric. Water Manag.* **2022**, *271*, 107763. [CrossRef]

29. Jaafar, H.; Mourad, R.; Hazimeh, R.; Sujud, L. AgSAT: A Smart Irrigation Application for Field-Scale Daily Crop ET and Water Requirements Using Satellite Imagery. *Remote Sens.* **2022**, *14*, 5090. [CrossRef]
30. Vanella, D.; Ramírez-Cuesta, J.M.; Intrigliolo, D.S.; Consoli, S. Combining electrical resistivity tomography and satellite images for improving evapotranspiration estimates of citrus orchards. *Remote Sens.* **2019**, *11*, 373. [CrossRef]
31. Mouazen, A.M.; Alhwaimel, S.A.; Kuang, B.; Waine, T. Multiple on-line soil sensors and data fusion approach for delineation of water holding capacity zones for site specific irrigation. *Soil Tillage Res.* **2014**, *143*, 95–105. [CrossRef]
32. Jain, S.; Vani, K.S. A survey of the automated irrigation systems and the proposal to make the irrigation system intelligent. *Int. J. Comput. Sci. Eng.* **2018**, *6*, 357–360. [CrossRef]
33. García, L.; Parra, L.; Jimenez, J.M.; Lloret, J.; Lorenz, P. IoT-based smart irrigation systems: An overview on the recent trends on sensors and IoT systems for irrigation in precision agriculture. *Sensors* **2020**, *20*, 1042. [CrossRef]
34. Zinkernagel, J.; Maestre-Valero, J.F.; Seresti, S.Y.; Intrigliolo, D.S. New technologies and practical approaches to improve irrigation management of open field vegetable crops. *Agric. Water Manag.* **2020**, *242*, 106404. [CrossRef]
35. Millán, S.; Casadesús, J.; Campillo, C.; Moñino, M.J.; Prieto, M.H. Using soil moisture sensors for automated irrigation scheduling in a plum crop. *Water* **2019**, *10*, 2061. [CrossRef]
36. Fernández, J.E.; Alcon, F.; Diaz-Espejo, A.; Hernandez-Santana, V.; Cuevas, M.V. Water use indicators and economic analysis for on-farm irrigation decision: A case study of a super high density olive tree orchard. *Agric. Water Manag.* **2020**, *237*, 106074. [CrossRef]
37. Panigrahi, P.; Raychaudhuri, S.; Thakur, A.K.; Nayak, A.K.; Sahu, P.; Ambast, S.K. Automatic drip irrigation scheduling effects on yield and water productivity of banana. *Sci. Hortic.* **2019**, *257*, 108677. [CrossRef]
38. Maqsood, H.; Hunsaker, D.J.; Waller, P.M.; Thorp, K.R.; French, A.; Elshikha, D.E.; Loeffler, R.L. WINDS Model Demonstration with Field Data from a Furrow-Irrigated Cotton Experiment. *Water* **2023**, *15*, 1544. [CrossRef]
39. Richards, L.A. Capillary conduction of liquids through porous mediums. *Physics* **1931**, *1*, 318–333. [CrossRef]
40. Elshikha, D.E.; Hunsaker, D.J.; Waller, P.M.; Thorp, K.R.; Dierig, D.A.; Wang, G.; Cruz, M.V.; Katterman, M.E.; Bronson, K.F.; Wall, G.W.; et al. Estimation of direct-seeded guayule growth, crop coefficient and yield parameters using UAS-based multispectral and RGB data. *Agric. Water Manag.* **2022**, *265*, 107540. [CrossRef]
41. Wang, G.S.; Elshikha, D.M.; Katterman, M.E.; Sullivan, T.; Dittmar, S.; Cruz, M.V.; Hunsaker, D.J.; Waller, P.M.; Ray, D.T.; Dierig, D.A. Irrigation effects on seasonal growth and rubber production of direct-seeded guayule. *Ind. Crops Prod.* **2022**, *177*, 114442. [CrossRef]
42. Brown, P.W. *Accessing the Arizona Meteorological Network (AZMET) by Computer, Extension Report. No. 8733*; University of Arizona: Tucson, AZ, USA, 1989.
43. Allen, R.G.; Walter, I.A.; Elliot, R.L.; Howell, T.A.; Itenfisu, D.; Jensen, M.E.; Snyder, R.L. (Eds.) *The ASCE Standardized Reference Evapotranspiration Equation*; American Society of Civil Engineers: Reston, VA, USA, 2005.
44. Post, D.F.; Mack, C.; Camp, P.D.; Sulliman, A.S. Mapping and characterization of the soils on the University of Arizona Maricopa Agricultural Center. In *Hydrology and Water Resources in Arizona and the Southwest*; University of Arizona: Tucson, AZ, USA, 1988; pp. 49–60.
45. Thorp, K.; Dierig, D.A. Color image segmentation approach to monitor flowering in lesquerella. *Ind. Crops Prod.* **2011**, *34*, 1150–1159. [CrossRef]
46. Tucker, C.J. Red and photographic infrared linear combinations for monitoring vegetation. *Remote Sens. Environ.* **1979**, *8*, 127–150. [CrossRef]
47. Schaap, M.G.; Leij, F.J.; Van Genuchten, M.T. Rosetta: A computer program for estimating soil hydraulic parameters with hierarchical pedotransfer functions. *J. Hydrol.* **2001**, *251*, 163–176. [CrossRef]